

Spatio-temporal Early Prediction based on Multi-objective Reinforcement Learning

Wei Shao*
Data61, CSIRO
Clayton, Victoria, Australia
phdweishao@gmail.com

Yufan Kang*
RMIT University
Melbourne, Victoria, Australia
yufan.kang@student.rmit.edu.au

Ziyan Peng
Xidian University
Xi'an, China

Xiao Xiao†
Xidian University
Xi'an, China
xiaoxiao@xidian.edu.cn

Lei Wang
Zhejiang University
Hangzhou, China

Yuhui Yang
Xidian University
Xi'an, China

Flora D. Salim
University of New South Wales
Sydney, Australia

ABSTRACT

Accuracy and timeliness are indeed often conflicting goals in prediction tasks. Premature predictions may yield a higher rate of false alarms, whereas delaying predictions to gather more information can render them too late to be useful. In applications such as wildfires, crimes, and traffic jams, timely predictions are vital for safeguarding human life and property. Consequently, finding a balance between accuracy and timeliness is crucial. In this paper, we propose a spatio-temporal early prediction model based on Multi-Objective reinforcement learning that can either implement an optimal policy given a preference or infer the preference based on a small number of samples. The model addresses two primary challenges: 1) enhancing the accuracy of early predictions and 2) providing the optimal policy for determining the most suitable prediction time for each area. Our method demonstrates superior performance on three large-scale real-world datasets, surpassing existing methods in early spatio-temporal prediction tasks.

CCS CONCEPTS

• **Computing methodologies** → **Neural networks; Spatial and physical reasoning;** • **Applied computing** → **Forecasting.**

KEYWORDS

Spatio-temporal data, Graph neural network, Early prediction, Responsible AI

*authors contributed equally to this research.

†Corresponding Author

Permission to make digital or hard copies of all or part of this work for personal or classroom use is granted without fee provided that copies are not made or distributed for profit or commercial advantage and that copies bear this notice and the full citation on the first page. Copyrights for components of this work owned by others than the author(s) must be honored. Abstracting with credit is permitted. To copy otherwise, or republish, to post on servers or to redistribute to lists, requires prior specific permission and/or a fee. Request permissions from permissions@acm.org.
Conference acronym 'XX, June 03–05, 2018, Woodstock, NY

© 2018 Copyright held by the owner/author(s). Publication rights licensed to ACM.
ACM ISBN 978-1-4503-XXXX-X/18/06
<https://doi.org/XXXXXXXX.XXXXXXX>

ACM Reference Format:

Wei Shao, Yufan Kang, Ziyan Peng, Xiao Xiao, Lei Wang, Yuhui Yang, and Flora D. Salim. 2018. Spatio-temporal Early Prediction based on Multi-objective Reinforcement Learning. In *Proceedings of Make sure to enter the correct conference title from your rights confirmation email (Conference acronym 'XX)*. ACM, New York, NY, USA, 10 pages. <https://doi.org/XXXXXXXX.XXXXXXX>

1 INTRODUCTION

Spatio-temporal prediction, an innovative intersection of geographic information systems, statistics, and data science, plays a pivotal role in fields where spatial distribution and temporal progression dictate outcomes. This predictive approach finds wide-ranging applications in domains such as meteorology, epidemiology, traffic control, parking, and urban planning [15, 19, 27, 29, 33, 35].

Spatio-temporal early prediction focuses on anticipating future events by examining patterns that change over space and time as early as possible, which is essential to many real-world applications such as epidemiology, environmental studies, and public safety, where early detection can lead to better management or prevention outcomes. For instance, within the context of forecasting the spread of diseases, the timeliness of predictions is considerably more critical than their accuracy. Forecasts that are accurate but delayed can lead to the unnecessary loss of thousands of lives. On the other hand, a prediction that is approximately accurate but made in a timely manner can significantly reduce the impact, saving lives.

Figure 1 shows that existing approaches to predicting spatio-temporal events are categorised into three distinct strategies: Traditional, Fixed, and Adaptive. For example, Hochreiter *et al.* [13] propose a traditional prediction method that considers the entire recorded data before the prediction. However, this approach can be time-consuming, particularly with large datasets, and its requirement for complete prior data collection often results in delayed predictions, which is unsuitable for time-sensitive applications. Conversely, Li's fixed early prediction approach operates within a set observation period [20], facilitating timely forecasts within a specific window. Although this strategy enhances promptness, its fixed timing can result in inaccuracies if the observation window is

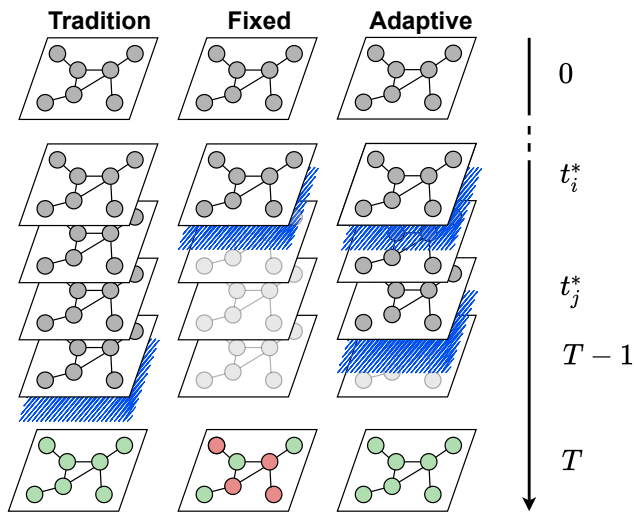


Figure 1: Example of three methods for early spatio-temporal prediction. Each circle is a node (e.g. sensor) with recorded value (such as speed) over time. The blue plane represents the prediction time, and the recorded values after the blue plane are not used for prediction. The adaptive early prediction method adjusts data usage and dynamically determines the prediction time for different nodes. The node colour at time T indicates the accuracy of prediction, green indicates that the predicted value matches the ground truth, and red indicates otherwise.

not optimally selected. Moreover, its rigidity in adjusting to temporal data variations and the risk of selection bias in determining the observation window could compromise prediction precision. The third approach, named adaptive early prediction, dynamically adjusts the prediction time based on data characteristics. This idea is inspired by Hartvigsen, who applied this idea in the time-series prediction area [11]. This innovative method aims to strike an optimal balance between prediction accuracy and timeliness, thereby attempting to optimise both the timeliness and accuracy of predictions. Its dynamic adaptability provides a significant edge in handling changes over time.

Although Hartvigsen has tried to apply the concept of early prediction in time-series area [11] and achieved some good results in the medical diagnosis, many challenges remain, especially in the spatio-temporal prediction. (1) **Real-time Bi-objective Balance in Highly Complex Environment:** Spatio-temporal data demand dynamic solutions, being more complex and subject to rapid changes than time-series data. Traditional multi-objective optimisation methods, which are static and computationally intensive, fail to adapt efficiently across different environments. At the same time, early prediction necessitates immediate results, as even a one-minute delay can lead to unfavourable outcomes. (2) **Spatio-temporal Comprehensive Dependency:** Relying solely on distance correlation for spatio-temporal predictions may fall short in quickly capturing essential data characteristics. Although distance correlation effectively reflects spatial connections among

nodes, it overlooks the crucial temporal aspects embedded within the data, which are vital for precise forecasting. (3) **Hidden Preferences Discovery:** The equilibrium between timeliness and accuracy varies across tasks, revealing diverse preferences. Identifying these subtle preferences is a complex challenge that demands a profound comprehension of the goals at hand and formulating an ideal balance between promptness and precision for each scenario. This highlights the necessity for refined and flexible strategies in spatio-temporal early prediction.

We address the aforementioned challenges by introducing a spatio-temporal early prediction model based on multi-objective reinforcement learning (STEMO). The key contributions of our study can be summarised as follows:

- We present a multi-objective reinforcement learning framework designed to optimise both the timeliness and accuracy of spatio-temporal predictions. This approach enhances adaptability to changing patterns through interactive learning from real-time feedback.
- We introduce a multiple-step similarity matrix, enabling each node to capture the trends from other upstream nodes so that we can estimate the changes of such nodes earlier.
- We develop a node embedding technique based on biased random walks, increasing the likelihood of visiting nodes with higher similarity and reaching the optimal time. To address the issue of non-uniform object scales or units, we devise a method to discover hidden preferences and employ the entropy weight method.

2 RELATED WORK

2.1 Spatio-temporal Prediction

It is evident that spatio-temporal prediction is of paramount importance in numerous real-world applications [31], such as weather prediction [2], traffic flow prediction [6], and earthquake prediction [37]. Traditional time-series methods, including ARIMA [1], have been extensively employed for prediction. With the evolution of machine learning, deep learning methods such as Long Short Term Memory (LSTM) [13] and Gate Recurrent Unit (GRU) [3] have demonstrated superior capabilities in capturing temporal correlations. Convolutional Neural Networks (CNNs) [18] are frequently utilised to capture spatial correlations in Euclidean space, whereas Graph Convolution Networks (GCNs) [17] serve to model non-Euclidean relationships among nodes. Despite these advancements, fixed observation windows limit the ability of these models to adjust their predictions in response to evolving data patterns, which could compromise their timeliness and accuracy, especially when dealing with rapidly changing data sources like traffic flow.

2.2 Early Prediction

Early prediction methods are techniques employed to make predictions based on specific identifiable characteristics or temporal patterns within a dataset. These methods can be classified into two categories: shapelet-based methods and predictor-based methods. Shapelet-based methods [7, 12] involve finding small sub-parts of the time series data, known as shapelets [36], that can be utilised for prediction. Predictor-based methods [8, 22, 23, 28] involve combining a set of predictors built at different points in time with one

or more conditions or trigger functions to evaluate the reliability of predictions and help determine whether they should be considered or discarded. Most of these methods prioritise accuracy over timeliness, inadvertently downplaying the role of prompt predictions. Some methods [22, 23, 30] allow for adjusting the trade-off between accuracy and timeliness with parameters, but these parameters can be difficult to adjust in advance and may require executing the algorithm multiple times to obtain solutions with different trade-offs. In this paper, we propose a Spatio-Temporal Early Prediction model that seeks to improve both the timeliness and accuracy of spatio-temporal predictions, addressing some of the limitations inherent in existing techniques.

3 PROBLEM DEFINITION

Consider a graph $\mathcal{G} = \{\mathbf{V}, \mathbf{E}\}$, where $\mathbf{V} = \{v_i\}_{i=1}^n$ denotes the set of nodes and $\mathbf{E} = \{e_{ij}\}_{i,j=1}^n$ represents the set of edges. The adjacency matrix $\mathbf{A} \in \mathbb{R}^{n \times n}$ captures the relationships (e.g., distance) between nodes. Recorded values $\mathbf{X}_t = \{x_t^i\}_{i=1}^n$ refer to the measurements obtained from the nodes at time t . Predicted values $\widehat{\mathbf{X}}_T = \{\hat{x}_T^i\}_{i=1}^n$ are the estimates of the values at time T based on the graph neural network model. For instance, in a traffic speed prediction scenario, x_t^i could be the speed at sensor v_i at time t , and \hat{x}_T^i could be the predicted speed at time T . The optimal time series $\mathbf{t}^* = \{t_i^*\}_{i=1}^n$ can guide the data observation process. For each node v_i , the corresponding optimal time t_i^* is the most appropriate prediction time such that the prediction accuracy is maximised and the time cost minimises. We aim to find the optimal time series that balances prediction accuracy and time cost. The optimal time for node v_i is computed using the following expression:

$$t_i^* = \arg \max_t \left(\log P(\hat{x}_T^i | \mathbf{X}_{0:t}, \mathcal{G}) - \text{Cost}(t) \right). \quad (1)$$

s.t. $t \in [0, T - 1]$

The objective function $\log P(\hat{x}_T^i | \mathbf{X}_{0:t}, \mathcal{G})$ denotes the log-likelihood of the predicted value given the past measurements and the graph structure, which can be seen as a measure of prediction accuracy. The function $\text{Cost}(t)$ represents the time cost of collecting records up to time t , and it is assumed to be monotonically increasing as more data is often more expensive to obtain.

4 METHODOLOGY

As shown in Figure 2, the Spatio-Temporal Early Prediction model based on Multi-Objective reinforcement learning (STEMO) consists of three main components: a spatio-temporal predictor, a state generator, and optimal policies for determining the optimal time. In addition, we also introduce how to find hidden preferences.

4.1 The Spatio-temporal Predictor

The main difference between traditional GCN and the Multi-Graph Convolutional Neural network (MGCN) is the addition of multiple time steps in the similarity matrix calculation in the latter. A standard GCN calculates similarity based on spatial proximity or a single time-point temporal similarity, leading to a limitation in capturing time-evolving trends. MGCN improves this by including multiple time-step similarities, capturing more intricate time-evolving correlations, and facilitating early prediction.

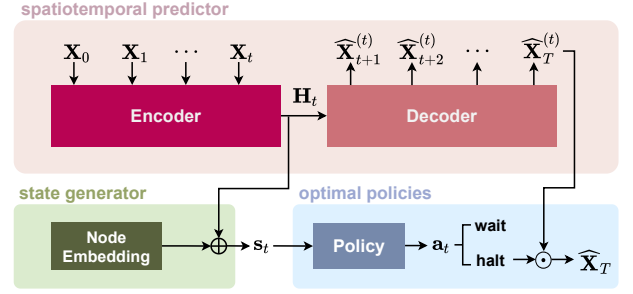


Figure 2: At time t , the encoder processes the recorded values $\mathbf{X}_{0:t}$ to extract spatio-temporal features and generate the hidden state \mathbf{H}_t . Using \mathbf{H}_t , the decoder generates a series of predicted values, focusing on $\widehat{\mathbf{X}}_T^{(t)}$. The state generator concatenates the node embedding result and \mathbf{H}_t to generate the state s_t . The policy utilises s_t to determine the optimal time for each node $v_i \in \mathbf{V}$ via the action set $\mathbf{a}_t = \{a_t^i\}_{i=1}^n$ (halt or wait). 'Wait' implies that further observation of recorded values is necessary, while 'Halt' implies that time t is the optimal time t_i^* for node v_i , and the corresponding predicted value is recorded in the predicted value $\widehat{\mathbf{X}}_T$.

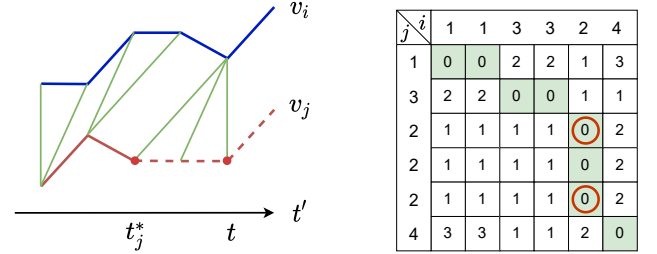


Figure 3: (a) Time series of nodes v_i and v_j . The dotted line represents the series after the optimal time. (b) DTW distance between the time series of nodes v_i and v_j .

Figure (a) shows the time series of nodes v_i and v_j . The dotted line represents the series after the optimal time, and we only need to observe the solid line to make prediction. The two solid dots in Figure (a) correspond to the two red circles in Figure (b). Take the red circle below as an example, it corresponds to the DTW distance between $x_{0:t}^i$ and $x_{t_j^*}^j$, which is calculated along the green grid path. We anticipate that node i will acquire feature $x_{t_j^*}^j$ at time t through MGCN, allowing it to make more precise predictions earlier.

Specifically, GCN collects equal-length time series of each node, applies the DTW algorithm to each pair of time series data, and uses dynamic time warping (DTW) distance [24] to create a similarity matrix. DTW is a method that finds an optimal match between two given sequences (e.g., time series) with certain restrictions, which is particularly useful in our setting where we seek to find correlations in temporal data. However, GCN has certain limitations. One limitation is that it does not consider the influence of other nodes

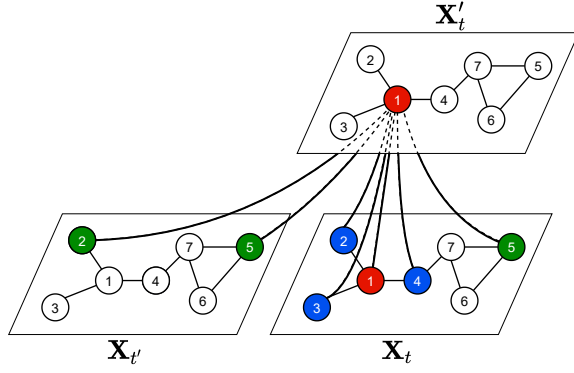


Figure 4: We assume node 1 (red) is the central node. The blue nodes represent spatially close nodes, while the green nodes represent temporally similar nodes. MGCN considers these two kinds of nodes, where spatial and temporal similarities are processed separately but in conjunction.

before time t . As shown in Figure 3, t represents a specific time, and t' is an arbitrary time. If $t' < t$ and $\text{DTW}(x_{0:t'}^j, x_t^i) = 0$, this may result from node v_j changing faster than the node v_i . In such cases, it would be advantageous for node v_i to incorporate the feature of node v_j at time t' in its prediction, as this would enable it to capture the changing trend better and facilitate early prediction. Moreover, if $t' = t_j^* < t$, this would also allow node i to reach the optimal time more quickly. Another limitation of this approach is that it may produce inaccurate results when $\text{DTW}(x_{t_j^*}^j, x_t^i) > 0$, indicating a weak correlation between nodes v_j and v_i . This may not always be true and could lead to sub-optimal predictions. The MGCN addresses these limitations, which is designed to optimize both prediction accuracy and prediction timing. As depicted in Figure 4, the multiple timesteps similarity matrix allows the model to capture correlations better, thus achieving more accurate prediction. In addition, MGCN can incorporate the fast-changing trends from other nodes to make predictions earlier.

The distance matrix $\mathbf{A}^S \in \mathbb{R}^{n \times n}$ is calculated according to the geometric distance between nodes:

$$\mathbf{A}_{i,j}^S = \begin{cases} \exp\left(-\frac{d_{ij}^2}{\eta^2}\right), & i \neq j \\ 0, & i = j \end{cases}, \quad (2)$$

where d_{ij} represents the distance between v_i and v_j , and η is the parameter that controls the distribution of \mathbf{A}^S .

The multiple timesteps similarity matrix $\mathcal{A}_{t,t'}^T \in \mathbb{R}^{(t+1) \times n \times n}$ is computed according to the temporal similarity between nodes:

$$\mathcal{A}_{t,t',i,j}^T = \begin{cases} e^{-\kappa \times \text{DTW}(x_{0:t'}^i, x_{0:t'}^j)} & i \neq j \\ 0 & i = j \end{cases}, \quad (3)$$

where κ controls the range of DTW distance and should be set based on the range of relevant conditions.

$$\mathbf{X}'_t = \sigma\left(\sum_{t'=0}^t \mathcal{A}_{t,t'} \mathbf{X}_{t'} \mathcal{W}_{t'}\right) \quad (4)$$

$$\mathbf{A}_{t,t'} = \begin{cases} \mathbf{A}_{t,t'}^T & t' \leq t \\ (\hat{\mathbf{A}}^S + \mathbf{A}_{t,t}^T)/2 & t' = t \end{cases}$$

where $\hat{\mathbf{A}}^S = \tilde{\mathbf{D}}^{-\frac{1}{2}} \tilde{\mathbf{A}}^S \tilde{\mathbf{D}}^{-\frac{1}{2}}$ represents pre-processing step, $\tilde{\mathbf{A}}^S = \mathbf{A}^S + \mathbf{I}$ is the matrix with added self-connections, \mathbf{I} is the identity matrix, $\tilde{\mathbf{D}} = \sum_j \tilde{\mathbf{A}}_{i,j}^S$ is degree matrix, $\sigma(\cdot)$ represents the sigmoid function, $\mathcal{W}_{t'} \in \mathbb{R}^{1 \times h}$ is learnable parameters with number of hidden unit h .

The encoder-decoder structure is utilized for its capacity to capture temporal dependencies and handle variable length sequences, as shown in Figure 2. In contrast to previous work, the variation in the number of prediction units (consisting of an MGCN and a GRU) allows the model to dynamically adjust its focus to different parts of the time sequence. At time t , the encoder has $t + 1$ prediction units. The recorded values \mathbf{X}_t are input into MGCN of the last prediction unit in the encoder and the result of graph convolution process \mathbf{X}'_t is then used as input for the GRU. Combining the hidden state \mathbf{H}_{t-1} of GRU output in the previous unit, the GRU outputs hidden state \mathbf{H}_t . In practice, in the encoder, only the last prediction unit at each time needs to be calculated. At time t , the decoder has $T - t - 1$ prediction units, and the last prediction unit outputs the candidate predicted values $\hat{\mathbf{X}}_T^{(t)}$.

$\hat{\mathbf{X}}_T^{(t)} = \mathbf{W} \mathbf{H}_T^{(t)} + \mathbf{b}$ represents candidate predicted values at time T predicted at time t , where \mathbf{W} and \mathbf{b} are learnable parameters. The spatio-temporal predictor is trained by minimizing the mean absolute error between $\hat{\mathbf{X}}_T$ and \mathbf{X}_T , where predicted values $\hat{\mathbf{X}}_T = \sum_{t=0}^{T-1} \mathbf{a}_t \odot \hat{\mathbf{X}}_T^{(t)}$, and \odot denotes the Hadamard product calculation.

4.2 State Generator

The relationship between nodes is based on temporal similarity and spatial similarity. In essence, if $x_{t'}^i$ and x_t^j show similarity, it suggests a possible temporal connection between node i and j . We propose to leverage this connection to help node j reach its optimal time more quickly by learning from node i . We designed an embedding function $f_t(\cdot)$ for each time t , which operates on the features of the node and aims to create a representation of each node at time t . The state s_t^i captures the current information status of node i at time t . It combines the hidden state $\mathbf{H}_t^i \in \mathbb{R}^h$ outputted by the encoder and the node embedding $f_t(v_i) \in \mathbb{R}^e$. The state is used to verify the optimal time by providing comprehensive information for each node at each time.

The choice of objective function stems from the assumption that a node's state is influenced by its neighbours' states, and the optimisation goal is to maximise the probability of the appearance of the node's neighbours given the node itself:

$$\max_{f_t} \sum_{v_i \in \mathbf{V}} \log Pr(N(v_i) | f_t(v_i)), \quad (5)$$

where $N(v_i)$ represents the set of neighbors of v_i obtained by biased random walk sampling [9, 25].

Biased random walk sampling is used to select a node's neighbours that contribute to its state. The bias term $\alpha_{pq}(t)$ and the transition probability $\min_{t'} \mathcal{A}_{t,t'}^T$ control the sampling process, favouring nodes that are closer (in terms of reaching their optimal time) and thus more relevant to the early prediction task. Given the source node v_i and the current node v_j , the probability of accessing the next node v_k is represented by the bias term $\alpha_{pq}(t)$ multiplied by the transition probability $\min_{t'} \mathcal{A}_{t,t'}^T$, where α represent bias, and is calculated as follows:

$$\alpha_{pq}(t) = \begin{cases} \frac{1}{p} & \text{if } v_k = v_i \\ \frac{1}{q} & \text{if } t_k^* \leq t \\ 1 & \text{else} \end{cases}, \quad (6)$$

where p controls the probability of revisiting the traversed node, and q controls the search program to distinguish whether the node reaches the optimal time or not. After the random walk sampling, the remaining steps are the same as in the DeepWalk [26] algorithm, using the word2vec [4] method to learn the embedding function $f_t(\cdot)$. In essence, nodes are treated as 'words' and node sequences sampled from random walks are treated as 'sentences'. By feeding these sequences into a word2vec model, we can learn an embedding for each node that captures its context within the graph, i.e., its neighbourhood structure.

4.3 Finding the Optimal Set of Policies

Since our goal is to induce a single model that can adapt to the entire space of preferences Ω (a set of different ways decision-makers can prioritise or value the various objectives involved in an optimisation problem), we use a neural network to represent the Q-values $Q \subseteq (\Omega \rightarrow \mathbb{R}^2)^{\mathcal{S} \times \mathcal{A}}$ with state space \mathcal{S} and action space \mathcal{A} . The input to this neural network is a concatenation of the states, actions, and user preferences. At time t , the network takes the states \mathbf{s}_t and preferences $\omega \in \Omega$ as input. We estimate the actions \mathbf{a}_t that maximise the output of the network and verify a series of optimal times according to the actions.

We use ε -greedy action selection to avoid abundant exploitation as follows:

$$\mathbf{a}_t = \begin{cases} \max_{\mathbf{a}} \omega^T \mathbf{Q}(\mathbf{s}_t, \mathbf{a}, \omega; \theta), & \text{w.p. } 1 - \varepsilon \\ \text{random}, & \text{w.p. } \varepsilon \end{cases}, \quad (7)$$

where θ indeed refers to the parameters of the Q-network, which are updated during training, action $\mathbf{a}_t = \{a_t^i\}_{i=1}^n$ is replaced by a random action with probability ε , and ε decreases exponentially from 1 to 0 during training. For node v_i , $a_t^i = 1$ indicates that t is the optimal time t_i^* . If $a_t^i = 0$, $t \in [0, T-1]$, time $T-1$ is the optimal time.

We designed reward $\mathbf{r}_t = \{r_{t,\text{acc}}^i, r_{t,\text{time}}^i\}_{i=1}^n$ includes accuracy reward and temporal reward. The accuracy reward reflects how well the current prediction and action align with the ground truth, while the temporal reward encourages faster convergence to the optimal time by penalising longer observation time. The specific calculation is as follows:

$$r_{t,\text{acc}}^i = -|\widehat{x}_T^i - x_T^i|, \quad r_{t,\text{time}}^i = -\rho t, \quad (8)$$

where ρ is the trade-off parameter.

To train the deep neural network, we minimise the following loss function at each step k :

$$L^A(\theta) = \mathbb{E}_{\mathbf{s}_t, \mathbf{a}_t, \omega} [\|\mathbf{y} - \mathbf{Q}(\mathbf{s}_t, \mathbf{a}_t, \omega; \theta)\|_2^2] \\ \mathbf{y} = \mathbf{r}_t + \gamma \arg \max_{\mathbf{a}, \omega'} \omega'^T \mathbf{Q}(\mathbf{s}_{t+1}, \mathbf{a}, \omega'; \theta_k). \quad (9)$$

The arg max operation is used to select the action and preference that maximise the future expected total rewards. However, the optimal frontier contains a large number of discrete policies, which makes the landscape of the loss function non-smooth. To address this problem, we use an auxiliary loss function:

$$L^B(\theta) = \mathbb{E}_{\mathbf{s}_t, \mathbf{a}_t, \omega} [|\omega^T \mathbf{y} - \omega^T \mathbf{Q}(\mathbf{s}_t, \mathbf{a}_t, \omega; \theta)|], \quad (10)$$

The final loss function is $L(\theta) = (1 - \lambda)L^A(\theta) + \lambda L^B(\theta)$, where λ is the weight that controls the trade off L^A and L^B . The value of λ is increased gradually from 0 to 1 during training.

Algorithm 1 Training of STEMO.

Input: distance matrix \mathbf{A}^S , a preference sampling distribution \mathcal{D} , path p_λ for the weight λ increasing from 0 to 1. Initialise encoder, decoder, node embedding $f(v_i)$ for $v_i \in \mathbf{V}$, network \mathbf{Q} .

Parameter: corresponding learnable parameters $\theta_e, \theta_d, \theta_f$, and θ .

Output: learned model

- 1: **repeat**
 - 2: initialized \mathbf{H}_{-1} for encoder. Sample a linear preference $\omega \sim \mathcal{D}$
 - 3: **for** $t = 0, \dots, T - 1$ **do**
 - 4: Observe recorded values \mathbf{X}_t .
 - 5: $\mathbf{H}_t = \text{Encoder}(\mathbf{X}_t, \mathcal{H}_{t-1}, \mathcal{A}^S; \theta_e)$.
 - 6: $\mathbf{s}_t^i = \mathbf{H}_t || f_t(v_i; \theta_f)$, for all $v_i \in \mathbf{V}$.
 - 7: $\mathbf{a}_t = \begin{cases} \max_{\mathbf{a}} \omega^T \mathbf{Q}(\mathbf{s}_t, \mathbf{a}, \omega; \theta), & \text{w.p. } 1 - \varepsilon \\ \text{random}, & \text{w.p. } \varepsilon \end{cases}$.
 - 8: update θ_f according to equation 5.
 - 9: initialized go symbol for the decoder.
 - 10: $\widehat{\mathbf{X}}_T^{(t)} = \text{Decoder}(\mathbf{H}_t, \mathcal{A}^S; \theta_d)$.
 - 11: **if** update network **then**
 - 12: Sample N_ω preferences $\{\omega_i \sim \mathcal{D}\}$.
 - 13: Compute y_i for all $1 \leq i \leq N_\omega$ according to equations 9.
 - 14: update parameters θ by descending its stochastic gradient $\nabla_\theta L(\theta)$ according to equations 9 and 10:
 - 15: Increase λ along the path p_λ .
 - 16: **end if**
 - 17: **end for**
 - 18: $\widehat{\mathbf{X}}_T = \sum_{t=0}^{T-1} \mathbf{a}_t \odot \widehat{\mathbf{X}}_T^{(t)}$
 - 19: update parameters θ_e and θ_d by descending its stochastic gradient according to MAE $(\mathbf{X}_T, \widehat{\mathbf{X}}_T)$.
 - 20: **until** stopping criteria is met.
-

4.4 Finding the Hidden Preference

Inspired by [34], we employ the hidden preference ω , which can greatly influence the policy's decisions. Given that only scalar rewards, $Y \in \mathbb{R}^{m \times 2}$ are available, where m represent the sample size,

and Y_{ij} represent reward of the object j in sample i . We propose that the preference follows a truncated multivariate Gaussian distribution $\mathcal{D}(\mu_1, \mu_2; \beta_1 \sigma, \beta_2 \sigma)$, where the non-negative parameters μ_1, μ_2 are the means with $\mu_1 + \mu_2 = 1$, σ is the standard deviation, and β is the weight indicating the significance of each reward.

We first normalise the rewards to Y'_{ij} and then convert these to variation sizes p_{ij} , enabling uniformity and standardisation of rewards. Subsequently, we calculate the information entropy E_j , which quantifies uncertainty in the reward distribution. The weight for object j , β_j , is derived from E_j , where a lower entropy, suggesting more predictability, results in a higher weight. The weight is calculated as follows:

$$Y'_{ij} = \frac{Y_{ij} - \min(Y_j)}{\max(Y_j) - \min(Y_j)}, p_{ij} = \frac{Y'_{ij}}{\sum_{i=1}^m Y'_{ij}} \quad (11)$$

$$E_j = -\frac{\sum_{i=1}^m p_{ij} \ln p_{ij}}{\ln m}, \beta_j = \frac{1 - E_j}{2 - \sum E_j}$$

In our endeavor to estimate the parameters of this Gaussian distribution, we combine the strength of policy gradient and random search. These strategies collectively aim to maximize the expected return in the target task, while maintaining the network parameters constant. This delicate balance is mathematically captured as:

$$\arg \max_{\mu_1, \mu_2} \mathbb{E}_{\omega \sim \mathcal{D}} \left(\mathbb{E}_{\mathbf{s}_t, \mathbf{a}_t} \left(\sum_{t=0}^{T-1} \mathbf{r}_t \right) \right) \quad (12)$$

5 EXPERIMENT

In this section, we mainly introduce the datasets, baselines and specific parameter settings, etc. Experiments were conducted around comparing the predicted performance of the Spatio-Temporal Early Prediction model based on Multi-Objective reinforcement learning (STEMO) against baselines, analyzing the effect of each module, and finding the hidden preference.

5.1 Experiment Settings

5.1.1 Datasets. We conduct experiments on three real-world large-scale datasets: **METR-LA** [14] The dataset used in this study is a collection of public transportation speed data from 207 sensors on the Los Angeles Expressway. The data was collected using ring detectors, and the sample rate is 5 minutes. The time range for the data is from March 1, 2012 to June 30, 2012. **EMS**¹ The emergency dataset used in this study is a collection of data from the New York Fire Department. The dataset contains 145 areas based on postal code and the sample rate is 1 hour. The recorded time range for the data is from January 1, 2011 to November 30, 2011. **NYPD**² The crime dataset used in this study is a collection of data from the New York Police Department. The dataset is divided into 77 regions based on administrative regions. The sample rate is 4 hours, and the recording time range is from January 1, 2014 to December 31, 2015.

Detailed statistics of the datasets are shown in Table 1. For NYPD, we take the centroid of the crime site in the area as the location

¹<https://data.cityofnewyork.us/Public-Safety/EMS-Incident-Dispatch-Data/76xm-jjuj>

²<https://www.kaggle.com/datasets/mrmorj/new-york-city-police-crime-data-historic>

Table 1: Statistics of datasets used in the experiments

Datasets	Samples	Nodes	Interval
METR-LA	34272	207	5min
EMS	7992	145	1h
NYPD	4386	77	4h

coordinates of the area. For METR-LA, NYPD and EMS, 70% of the data are used for training, 20% for testing, and the rest 10% for verification. The proposed model is executed on a Windows system with Nvidia GeForce RTX 3070Ti.

5.1.2 Parameters Settings. For our proposed model, we selected parameters based on preliminary experiments and prior research. Specifically, we adopted the Adam optimizer [16] with an initial learning rate of 0.001, which proved to offer a stable and efficient convergence in our preliminary experiments. We set the hidden state dimension h to 12 as it provided a good balance between computational complexity and model performance. Similarly, the batch size is set to 32. The number of preferences $N_\omega = 16$, the node embedding dimension $e = 4$, the parameter $\kappa = 0.005$. In addition, $p = 2$, $q = 0.5$, $\rho = 0.5$, and $T = 12$ are all inspired by prior work. The source code is available at <https://github.com/coco0106/MO-STEP>.

5.1.3 Baselines and Metrics. We compare STEMO with various baselines for spatio-temporal prediction tasks and early prediction tasks, including **HA** [21], **LSTM** [13], **DCRNN** [20], **ASTGCN** [10], **EARLIEST** [11], **Graph-WaveNet** [32].

5.1.4 Metrics. We use three popular prediction indicators to evaluate the performance of all models, including mean absolute error (MAE), root mean square error (RMSE), and mean absolute percentage error (MAPE), which are commonly used measures in regression tasks to evaluate the average magnitude of prediction errors.

In addition, we computed the hypervolume (HV) [38] and the spacing (S) [5] metrics, which are commonly used to evaluate the performance of multi-objective optimization algorithms. The HV metric measures the volume of the space dominated by the Pareto front found by the algorithm up to a reference point. A higher HV value means that the algorithm has found a set of solutions that dominate a larger part of the target space, which is usually better. S metric measures the distance between adjacent solutions in Pareto frontier. A lower S value is usually better, because it shows that the solutions are more evenly distributed and provide decision makers with a wider range of trade-off options.

$$HV = \bigcup_{\phi \in \Phi} V(\phi, \varphi), \quad (13)$$

where $V(\phi, \varphi)$ represents the hyper volume of the space formed between the solution ϕ and the reference point φ in the non-dominant solution set Φ , which is the volume of the hypercube constructed with the connecting line between the solution ϕ and the reference point φ as the diagonal, and the solution with the lowest accuracy and the largest time used percentage in the corresponding data set

Table 2: Performance comparison on the three datasets. The average used time percentage is calculated according to $\frac{100\%}{n} \sum_{i=1}^n t_i^*/T$. The optimal time of LSTM, DCRNN, and ASTGCN is a fixed value set in advance, which means that the model is not responsible for determining the optimal time.

Datasets	Average used time percentage	100%		75%		50%		25%	
		MAE	RMSE	MAE	RMSE	MAE	RMSE	MAE	RMSE
METR-LA	HA	7.22	9.46	7.22	9.46	7.22	9.46	7.22	9.46
	LSTM	4.99 ± 0.07	7.48 ± 0.07	7.17 ± 0.11	10.21 ± 0.10	7.50 ± 0.13	10.46 ± 0.11	7.72 ± 0.15	10.68 ± 0.17
	DCRNN	2.27 ± 0.06	3.94 ± 0.07	2.91 ± 0.08	5.76 ± 0.09	3.25 ± 0.10	6.68 ± 0.09	3.48 ± 0.11	7.23 ± 0.10
	ASTGCN	3.54 ± 0.16	7.39 ± 0.17	5.05 ± 0.18	6.48 ± 0.18	6.65 ± 0.20	12.70 ± 0.21	7.64 ± 0.23	14.40 ± 0.25
	EARLIEST	5.01 ± 0.08	7.46 ± 0.09	5.93 ± 0.10	8.21 ± 0.10	6.14 ± 0.11	9.26 ± 0.10	6.85 ± 0.12	10.06 ± 0.11
	Graph-WaveNet	2.38 ± 0.15	4.21 ± 0.08	3.22 ± 0.11	6.45 ± 0.09	3.81 ± 0.07	7.70 ± 0.08	4.35 ± 0.16	8.65 ± 0.1
	STEMO	2.23 ± 0.07	3.96 ± 0.06	2.37 ± 0.08	4.45 ± 0.08	3.23 ± 0.08	5.69 ± 0.09	3.49 ± 0.09	6.15 ± 0.09
EMS	HA	1.47	2.41	1.47	2.41	1.47	2.41	1.47	2.41
	LSTM	1.61 ± 0.04	2.63 ± 0.05	1.67 ± 0.04	2.78 ± 0.06	1.67 ± 0.07	2.79 ± 0.08	1.68 ± 0.08	2.78 ± 0.09
	DCRNN	1.45 ± 0.03	2.60 ± 0.03	1.69 ± 0.04	3.19 ± 0.05	1.58 ± 0.05	2.92 ± 0.05	1.70 ± 0.06	3.16 ± 0.07
	ASTGCN	1.49 ± 0.04	1.95 ± 0.03	1.78 ± 0.04	2.49 ± 0.05	1.85 ± 0.05	2.84 ± 0.06	2.01 ± 0.07	3.12 ± 0.08
	EARLIEST	1.62 ± 0.05	2.63 ± 0.06	1.64 ± 0.05	2.67 ± 0.06	1.66 ± 0.06	2.71 ± 0.06	1.68 ± 0.06	2.79 ± 0.07
	Graph-WaveNet	1.25 ± 0.07	2.42 ± 0.12	1.27 ± 0.09	2.46 ± 0.16	1.29 ± 0.11	2.48 ± 0.04	1.28 ± 0.06	2.49 ± 0.17
	STEMO	1.29 ± 0.02	2.23 ± 0.03	1.32 ± 0.03	2.32 ± 0.04	1.40 ± 0.03	2.41 ± 0.03	1.44 ± 0.03	2.49 ± 0.05
NYPD	HA	1.54	2.00	1.54	2.00	1.54	2.00	1.54	2.00
	LSTM	1.52 ± 0.04	2.16 ± 0.04	1.61 ± 0.05	2.29 ± 0.06	1.73 ± 0.07	2.40 ± 0.07	1.72 ± 0.08	2.40 ± 0.09
	DCRNN	1.58 ± 0.04	2.16 ± 0.04	1.60 ± 0.05	2.21 ± 0.05	1.61 ± 0.05	2.22 ± 0.06	1.66 ± 0.06	2.32 ± 0.07
	ASTGCN	2.18 ± 0.06	3.08 ± 0.12	2.88 ± 0.07	3.31 ± 0.13	2.99 ± 0.08	3.42 ± 0.13	3.69 ± 0.09	4.09 ± 0.14
	EARLIEST	1.52 ± 0.05	2.17 ± 0.05	1.59 ± 0.06	2.23 ± 0.07	1.64 ± 0.07	2.36 ± 0.07	1.65 ± 0.08	2.39 ± 0.09
	Graph-WaveNet	1.48 ± 0.08	2.05 ± 0.11	1.5 ± 0.06	2.08 ± 0.11	1.54 ± 0.15	2.14 ± 0.05	1.58 ± 0.08	2.18 ± 0.02
	STEMO	1.36 ± 0.03	1.82 ± 0.05	1.38 ± 0.04	1.97 ± 0.06	1.45 ± 0.06	2.12 ± 0.07	1.49 ± 0.07	2.27 ± 0.09

Table 3: Performance comparison on three datasets (HV and S metrics). ↑ means that the higher the metric value, the better the model performance, and ↓ means that the lower the metric value, the better the model performance.

Datasets	METR-LA		EMS		NYPD	
	HV↑	S↓	HV↑	S↓	HV↑	S↓
HA	3.71	-	0.56	-	1.57	-
LSTM	2.96	1.25	0.28	0.34	1.30	0.35
DCRNN	5.88	1.33	0.12	0.55	1.38	0.34
ASTGCN	2.41	1.77	0.26	0.59	0.36	0.53
EARLIEST	3.91	1.08	0.33	0.34	1.32	0.33
Graph-WaveNet	4.68	0.81	0.26	0.35	0.36	0.38
STEMO	6.73	0.71	0.58	0.34	1.47	0.36

is used as the reference point.

$$S = \sqrt{\frac{1}{|\Phi| - 1} \sum_{i=1}^{|\Phi|} (\bar{d} - d_i)^2}, \quad (14)$$

where d_i represents the minimum distance from the i^{th} solution to other solutions in Φ , and \bar{d} represents the average value of all d_i .

5.2 Experiment Results

We evaluate the performance of STEMO against the chosen baseline models in terms of the aforementioned metrics. The impact of

each module is quantified through an ablation study, where we sequentially remove one module at a time and measure the change in overall performance. In addition, we also reveal hidden preferences.

5.2.1 Performance Comparison. As shown in Table 2, we vary the average used time percentage by adjusting the preference, where the average usage time percentage, defined as the sum of the optimal time instances t_i^* for all n nodes divided by the total time period T and multiplied by 100%, represents the proportion of optimal time in the total time. This approach allows us to explore different prediction timeliness and assess the corresponding prediction accuracy, where the accuracy is measured by the error between the ground

Table 4: Some specific elements (the similarity matrix, node embedding, and policy) were excluded from the model and the resulting modified model’s performance was compared to that of the complete STEMO model.

Average used time percentage	100%			75%			50%			25%		
	MAE	RMSE	MAPE	MAE	RMSE	MAPE	MAE	RMSE	MAPE	MAE	RMSE	MAPE
w/o similarity matrix	1.38	1.98	5.21%	1.43	2.13	5.72%	1.50	2.28	6.32%	1.57	2.43	6.65%
w/o node embedding	1.36	1.84	4.92%	1.40	1.96	5.67%	1.49	2.06	5.74%	1.55	2.33	6.03%
w/o policy	1.36	1.83	4.91%	1.39	1.98	5.72%	1.52	2.74	6.43%	1.69	2.51	6.77%
STEMO	1.36	1.82	4.91%	1.38	1.97	5.01%	1.45	2.12	5.32%	1.49	2.27	5.84%

truth and the predicted values obtained by each node at their optimal time. We observe that: (1) When considering the same average used time percentage, the STEMO model exhibits higher accuracy compared to LSTM, DCRNN, ASTGCN, and Graph-WaveNet. The accuracy of the STEMO model shows a lesser decrease when the average usage time percentage experiences an equivalent reduction. This suggests that the STEMO model, which determines the optimal time based on the network’s dynamics, can adapt to diverse scenarios, striking a balance between timeliness and accuracy in predictions. In contrast, the fixed optimal time used by LSTM, DCRNN, ASTGCN, and Graph-WaveNet might not adequately account for the dynamic nature of various scenarios. (2) When the average used time percentage is the same, the STEMO model outperforms EARLIEST in terms of accuracy. This improvement can be attributed to the STEMO model’s consideration of spatial and temporal characteristics, especially in scenarios like the METRLA dataset, where the nodes are densely distributed and exhibit strong correlations. The STEMO model leverages a Multi-Graph Convolutional Neural network (MGCN) that incorporates multiple time-steps similarity matrices and the distance matrix. This framework effectively captures and utilises the spatio-temporal correlations among the nodes. Additionally, our experiments revealed that ASTGCN exhibits poor performance on the NYPD dataset. This outcome could be attributed to missing values within the dataset and the limited representation ability of the model.

As depicted in Table 3, above-average HV and lower S metrics for the STEMO model indicate its effectiveness in managing a trade-off between accuracy and timeliness in predictions - our primary objectives in this study. A higher HV, as observed in the STEMO model, signifies not only better convergence, illustrating the proximity of the solution set to the real Pareto frontier, but also greater extensiveness, indicating a broad coverage of the solution set in the objective space. Additionally, it implies better uniformity, showing an even distribution of individual solutions in the set. This high HV value affirms our assumption that the STEMO model can effectively balance prediction accuracy while maintaining the timeliness of predictions and offer a wide array of diverse solutions. On the other hand, the S metric provides a measure of the dispersion or spread of the solutions in the objective space. A lower S, as displayed by the STEMO model, suggests that the solutions are evenly distributed. This means that the STEMO model offers a variety of optimal times for predictions, and provides a robust and versatile model for various scenarios. This aligns well with our goal of creating a model that can cater to diverse situations with reliable results across a range of prediction times.

5.2.2 Ablation Study. To assess the contribution of individual components within our proposed STEMO model, we conducted an ablation study using the NYPD dataset, the results of which are presented in Table 4. In the ablation study, we evaluated the following variants of the STEMO model: **w/o similarity matrix** (without similarity matrix), **w/o node embedding** (without node embedding), **w/o policy** (without policy only use fixed value).

As seen from Table 4, the full STEMO model consistently outperforms all variants across different average used time percentages in terms of MAE, RMSE, and MAPE. For instance, when the similarity matrix is removed (‘w/o similarity matrix’), the performance degrades, especially at lower average used time percentages. This suggests the importance of the similarity matrix in capturing spatio-temporal information to maintain the model’s performance even at lower time percentages. The removal of the node embedding (‘w/o node embedding’) and the policy network (‘w/o policy’) also leads to a decrease in performance. This emphasizes the significance of the node embedding in capturing the spatial dependencies and the policy network in adaptively determining the optimal time for predictions. Overall, these findings underline the importance of each component and how they collectively contribute to the robust performance of the STEMO model in balancing prediction accuracy and timeliness.

5.2.3 Revealing hidden preferences. We modified the parameter ρ to provide vectorized rewards for encoding two different objects: timeliness and accuracy. We used two different tasks (g1, g2) and used only 100 episodes to learn the hidden preferences. The derived hidden preferences are depicted in Table 5. The learned preferences of the model are concentrated on the diagonal, indicating that they are in good agreement with the actual potential preferences. For variant g1, the model shows a strong preference (0.67) for timeliness. This result is consistent with the primary goal of g1, which emphasizes making predictions as quickly as possible. g2 primarily focuses on accuracy, as evidenced by the significantly higher preference weight (0.97) for accuracy.

Table 5: Derived preferences for timeliness and accuracy in the spatio-temporal early prediction model across two task variants (g1 and g2).

	timeliness	accuracy
g1	0.67	0.33
g2	0.02	0.97

6 DISCUSSION

Although the STEMO model shows promise in handling early spatio-temporal prediction tasks, several areas merit further exploration. First, the model's performance might be restricted if it was primarily validated on a limited set of real-world datasets, which brings into question its generalizability to different scenarios or data types. Future studies could benefit from testing the model on a more diverse datasets from varying domains. Second, the model's complexity might pose challenges in interpretation and computational efficiency. Third, future work should aim to simplify the model or increase its interpretability without sacrificing performance. Additionally, the model's ability to learn hidden preferences requires deeper investigation.

7 CONCLUSION

We propose the Spatio-Temporal Early Prediction model based on Multi-Objective reinforcement learning (STEMO) model, specifically designed to address challenges in early spatio-temporal prediction. The STEMO model leverages the Multi-Graph Convolutional Neural network (MGCN) and Gated Recurrent Unit (GRU) to capture and analyze spatio-temporal correlations. Further, it utilizes the hidden state from the encoder's output in conjunction with node embeddings to adaptively determine the optimal time for prediction. Additionally, we also explore hidden preferences within our model. Future work will focus on further refining our model, exploring its application in other domains, and addressing any limitations encountered in this study. We believe that our research contributes significantly to the ongoing discourse in the field of spatio-temporal prediction and will serve as a foundation for future advancements.

ACKNOWLEDGMENTS

We acknowledge the support of the Australian Research Council (ARC) Centre of Excellence for Automated Decision-Making and Society (ADM+S) (CE200100005). This research/project was undertaken with the assistance of computing resources from RACE (RMIT AWS Cloud Supercomputing) (RMAS00045). Flora Salim would also like to acknowledge edge the support of Cisco's National Industry Innovation Network (NIIN) Research Chair Program.

REFERENCES

- [1] Mohammed S Ahmed and Allen R Cook. 1979. *Analysis of freeway traffic time-series data by using Box-Jenkins techniques*.
- [2] Rafaela Castro, Yania M Souto, Eduardo Ogasawara, Fabio Porto, and Eduardo Bezerra. 2021. Stconvs2s: Spatiotemporal convolutional sequence to sequence network for weather forecasting. *Neurocomputing* 426 (2021), 285–298.
- [3] Kyunghyun Cho, Bart Van Merriënboer, Dzmitry Bahdanau, and Yoshua Bengio. 2014. On the properties of neural machine translation: Encoder-decoder approaches. *arXiv preprint arXiv:1409.1259* (2014).
- [4] Kenneth Ward Church. 2017. Word2Vec. *Natural Language Engineering* 23, 1 (2017), 155–162.
- [5] Kalyanmoy Deb and Sachin Jain. 2002. Running performance metrics for evolutionary multi-objective optimization. (07 2002).
- [6] Alireza Ermagun and David Levinson. 2018. Spatiotemporal traffic forecasting: review and proposed directions. *Transport Reviews* 38, 6 (2018), 786–814.
- [7] Mohamed F Ghalwash, Vladan Radosavljevic, and Zoran Obradovic. 2014. Utilizing temporal patterns for estimating uncertainty in interpretable early decision making. In *Proceedings of the 20th ACM SIGKDD international conference on Knowledge discovery and data mining*. 402–411.
- [8] Mohamed F Ghalwash, Dušan Ramljak, and Zoran Obradović. 2012. Early classification of multivariate time series using a hybrid HMM/SVM model. In *2012 IEEE International Conference on Bioinformatics and Biomedicine*. IEEE, 1–6.
- [9] Aditya Grover and J. Leskovec. 2016. node2vec: Scalable Feature Learning for Networks. *Proceedings of the 22nd ACM SIGKDD International Conference on Knowledge Discovery and Data Mining* (2016). <https://doi.org/10.1145/2939672.2939754>
- [10] Shengnan Guo, Youfang Lin, Ning Feng, Chao Song, and Huaiyu Wan. 2019. Attention based spatial-temporal graph convolutional networks for traffic flow forecasting. In *Proceedings of the AAAI conference on artificial intelligence*. AAAI Press, Honolulu, Hawaii, USA, 922–929.
- [11] Thomas Hartvigsen, Cansu Sen, Xiangnan Kong, and Elke Rundensteiner. 2019. Adaptive-halting policy network for early classification. In *Proceedings of the 25th ACM SIGKDD International Conference on Knowledge Discovery & Data Mining*. 101–110.
- [12] Guoliang He, Yong Duan, Rong Peng, Xiaoyuan Jing, Tiejun Qian, and Lingling Wang. 2015. Early classification on multivariate time series. *Neurocomputing* 149 (2015), 777–787.
- [13] Sepp Hochreiter and Jürgen Schmidhuber. 1997. Long short-term memory. *Neural computation* 9, 8 (1997), 1735–1780.
- [14] Hosagrahar V Jagadish, Johannes Gehrke, Alexandros Labrinidis, Yannis Papakonstantinou, Jignesh M Patel, Raghu Ramakrishnan, and Cyrus Shahabi. 2014. Big data and its technical challenges. *Commun. ACM* 57, 7 (2014), 86–94.
- [15] Maxwell B Joseph, Matthew W Rossi, Nathan P Mietkiewicz, Adam L Mahood, Megan E Cattau, Lise Ann St. Denis, R Chelsea Nagy, Virginia Iglesias, John T Abatzoglou, and Jennifer K Balch. 2019. Spatiotemporal prediction of wildfire size extremes with Bayesian finite sample maxima. *Ecological Applications* 29, 6 (2019), e01898.
- [16] Diederik P Kingma and Jimmy Ba. 2014. Adam: A method for stochastic optimization. *arXiv preprint arXiv:1412.6980* (2014).
- [17] Thomas N Kipf and Max Welling. 2016. Semi-supervised classification with graph convolutional networks. *arXiv preprint arXiv:1609.02907* 54, 4 (2016), 2645–2656.
- [18] Yann LeCun, Bernhard Boser, John S Denker, Donnie Henderson, Richard E Howard, Wayne Hubbard, and Lawrence D Jackel. 1989. Backpropagation applied to handwritten zip code recognition. *Neural computation* 1, 4 (1989), 541–551.
- [19] Fuxian Li, Jie Feng, Huan Yan, Guangyin Jin, Fan Yang, Funing Sun, Depeng Jin, and Yong Li. 2021. Dynamic graph convolutional recurrent network for traffic prediction: Benchmark and solution. *ACM Transactions on Knowledge Discovery from Data (TKDD)* (2021).
- [20] Yaguang Li, Rose Yu, Cyrus Shahabi, and Yan Liu. 2017. Diffusion convolutional recurrent neural network: Data-driven traffic forecasting. *arXiv preprint arXiv:1707.01926* (2017).
- [21] Jing Liu and Wei Guan. 2004. A summary of traffic flow forecasting methods [J]. *Journal of highway and transportation research and development* 3 (2004), 82–85.
- [22] Usue Mori, Alexander Mendiburu, Sanjoy Dasgupta, and Jose A Lozano. 2017. Early classification of time series by simultaneously optimizing the accuracy and earliness. *IEEE transactions on neural networks and learning systems* 29, 10 (2017), 4569–4578.
- [23] Usue Mori, Alexander Mendiburu, Eamonn Keogh, and Jose A Lozano. 2017. Reliable early classification of time series based on discriminating the classes over time. *Data mining and knowledge discovery* 31, 1 (2017), 233–263.
- [24] Meinard Müller. 2007. Dynamic time warping. *Information retrieval for music and motion* (2007), 69–84.
- [25] Duong Nguyen and Fragkiskos D. Malliaros. 2018. BiasedWalk: Biased Sampling for Representation Learning on Graphs. *2018 IEEE International Conference on Big Data (Big Data)* (2018), 4045–4053. <https://doi.org/10.1109/BigData.2018.8621872>
- [26] Bryan Perozzi, Rami Al-Rfou, and Steven Skiena. 2014. Deepwalk: Online learning of social representations. In *Proceedings of the 20th ACM SIGKDD international conference on Knowledge discovery and data mining*. 701–710.
- [27] Wei Shao, Zhiling Jin, Shuo Wang, Yufan Kang, Xiao Xiao, Hamid Menouar, Zhaofeng Zhang, Junshan Zhang, and Flora Salim. 2022. Long-term Spatio-Temporal Forecasting via Dynamic Multiple-Graph Attention. In *31st International Joint Conference on Artificial Intelligence, IJCAI 2022*. International Joint Conferences on Artificial Intelligence, 2225–2232.
- [28] Wei Shao, Ziyao Peng, Yufan Kang, Xiao Xiao, and Zhiling Jin. 2023. Early Spatiotemporal Event Prediction via Adaptive Controller and Spatiotemporal Embedding. In *2023 IEEE International Conference on Data Mining (ICDM)*. IEEE, 1307–1312.
- [29] Wei Shao, Yu Zhang, Pengfei Xiao, Kyle Kai Qin, Mohammad Saiedur Rahaman, Jeffrey Chan, Bin Guo, Andy Song, and Flora D Salim. 2024. Transferrable contextual feature clusters for parking occupancy prediction. *Pervasive and Mobile Computing* 97 (2024), 101831.
- [30] Romain Tavenard and Simon Malinowski. 2016. Cost-aware early classification of time series. In *Joint European conference on machine learning and knowledge discovery in databases*. Springer, 632–647.
- [31] Senzhang Wang, Jiannong Cao, and Philip S. Yu. 2022. Deep Learning for Spatio-Temporal Data Mining: A Survey. *IEEE Transactions on Knowledge and Data Engineering* 34, 8 (2022), 3681–3700. <https://doi.org/10.1109/TKDE.2020.3025580>
- [32] Zonghan Wu, Shirui Pan, Guodong Long, Jing Jiang, Xiaojun Chang, and Chengqi Zhang. 2019. Graph WaveNet for Deep Spatial-Temporal Graph Modeling. In

- Proceedings of the 28th International Joint Conference on Artificial Intelligence*. AAAI Press, 1907–1913.
- [33] Lianghao Xia, Chao Huang, Yong Xu, Peng Dai, Liefeng Bo, Xiyue Zhang, and Tianyi Chen. 2021. Spatial-Temporal Sequential Hypergraph Network for Crime Prediction with Dynamic Multiplex Relation Learning. In *IJCAI International Joint Conferences on Artificial Intelligence Organization*, 1631–1637.
- [34] Runzhe Yang, Xingyuan Sun, and Karthik Narasimhan. 2019. A generalized algorithm for multi-objective reinforcement learning and policy adaptation. *Advances in neural information processing systems* 32 (2019).
- [35] Suwei Yang, Massimo Lupascu, and Kuldeep S Meel. 2021. Predicting forest fire using remote sensing data and machine learning. In *Proceedings of the AAAI Conference on Artificial Intelligence*. arXiv, 14983–14990.
- [36] Lexiang Ye and Eamonn Keogh. 2009. Time series shapelets: a new primitive for data mining. In *Proceedings of the 15th ACM SIGKDD international conference on Knowledge discovery and data mining*. 947–956.
- [37] Daoye Zhu, Yi Yang, Fuhu Ren, Shunji Murai, Chengqi Cheng, and Min Huang. 2021. Novel Intelligent Spatiotemporal Grid Earthquake Early-Warning Model. *Remote Sensing* 13, 17 (2021), 3426.
- [38] E. Zitzler and L. Thiele. 1998. An evolutionary algorithm for multiobjective optimization: the strength Pareto approach, Vol. 43.

Received 20 February 2007; revised 12 March 2009; accepted 5 June 2009